

Dimension-Aware Neural Operator Learning

Yichen Song¹ Jiaming Wang¹ Yunbo Wang¹ Xiaokang Yang¹

Abstract

In the realm of computational physics, an enduring topic is the numerical solutions to partial differential equations (PDEs). Recently, the attention of researchers has shifted towards Neural Operator methods, renowned for their capability to approximate “operators”—mappings from functions to functions. Despite the universal approximation theorem within neural operators, ensuring error bounds often requires employing numerous Fourier layers. However, what about lightweight models? In response to this question, we introduce DimOL (Dimension-aware Operator Learning), drawing insights from dimensional analysis. To implement DimOL, we propose the ProdLayer, which can be seamlessly integrated into FNO/CNO-based and Transformer-based PDE solvers, enhancing their ability to handle sum-of-products structures inherent in many physical systems. Empirically, DimOL models achieve up to 48% performance gain within the PDE datasets. Furthermore, by analyzing Fourier components’ weights, we can symbolically discern the physical significance of each term. This sheds light on the opaque nature of neural networks, unveiling underlying physical principles.

1. Introduction

The Neural Operator methods have come to vision within the field of AI for science (AI4Sci), for their excellent property of having the ability to approximate any operators (*i.e.*, mapping from function space to another function space), while traditional neural networks would fail. However, are these models sufficiently “scientific” for AI4Sci research?

A recent work, F-FNO (Tran et al., 2023), has raised a crucial question about the performance of Neural Operator methods, particularly when models are expected to handle multiple background scenarios, such as varying viscosities in fluid dynamics problems. It demands a deeper understanding of the underlying physics. Nevertheless, the F-FNO paper does not fully address the raised issue: It lacks a comparative analysis of F-FNO model performance against other models, and notably, F-FNO itself does not

incorporate dimension awareness. Our research would reveal one simple but profound fact: *Models equipped with dimensional awareness tend to perform universally better.*

Accordingly, we propose Dimension-Aware Operator Learning (DimOL) to improve neural operators in handling physical quantities. Building upon the widely recognized physical intuition that quantities with different units (or dimensions) cannot be directly added but can be meaningfully multiplied, we implement DimOL using a simple yet novel network architecture that encodes product terms between channels. The proposed ProdLayer module is plug-and-play, making it easily applicable to a wide range of existing Neural Operators without significantly increasing the parameter count.

Notably, the dimensional awareness introduced by the ProdLayer is NOT merely about adding the product encodings to the base model. For example, in FNO-based models, replacing the linear transform in the Fourier domain with a ProdLayer does not yield improvement. This approach introduces a global convolution on the variable field, $\mathcal{F}^{-1}(\hat{f}\hat{g}) = f * g$, which does not hold physical significance in this context. Therefore, to adapt a model to incorporate DimOL, it is crucial to carefully consider the potential physical meaning of the model’s latent space. Another advantage of integrating dimensional awareness with operator learning—consistent with our scientific common sense—is its potential to reverse-engineer the meanings of latent variables and discover their symbolically meaningful relationships. This ability is also demonstrated through the experiments presented in this paper.

We evaluate our DimOL approach on classic physics simulation datasets, including regular mesh scenarios (*i.e.*, *Burgers*, *Darcy Flow*, and *Navier-Stokes*) and irregular mesh settings (*i.e.*, *Inductor2D*). Our empirical findings are as follows:

1. **Consistently improved PDE solvers:** We show that by integrating ProdLayer, existing neural operators, including FNO-based (Li et al., 2021; Tran et al., 2023; Kossaifi et al., 2023), Transformer-based (Wu et al., 2023), and kernel-convolution-based (Raonic et al., 2024) models, all present improved performance, particularly as the diversity of input physical quantities increases. For instance, on the TorusVisForce dataset proposed by F-FNO (which includes three physical quantities), our DimOL models reduce the prediction error by up to 48% com-

pared to the baseline models.

2. **Strong few-shot learning ability:** Another way to investigate the benefits of incorporating dimensional awareness is to train the model in few-shot learning setups. Specifically, we evaluate the model’s performance on transformed test data with linearly scaled physical coefficients. In this setup, the task would be challenging if the model treats it as an out-of-distribution (OOD) generalization problem, but it becomes easier if the model can uncover the hidden physical law behind the few-shot observed data. DimOL demonstrates significant advantages over the baseline models, making accurate predictions despite the few-shot learning scenario.

3. **Generalization well to new boundary conditions.** DimOL demonstrates strong generalization performance on CylinderFlow scenes with new test boundaries. In these experiments, the models are trained on data with various cylinder shapes and tested on OOD data with unseen combinations of the training cylinders. Our approach generalizes well to the unseen combined boundaries, which is challenging due to the complex flow reflections that may arise from multiple cylinders.

4. **Ablation studies.** We empirically compare the ProdLayer with alternative implementations of DimOL, such as the Quadratic layer, which could theoretically serve similar purposes. Our findings show that the proposed ProdLayer delivers the best performance, striking a good balance between effectiveness and simplicity.

2. Related Work

2.1. Numerical PDE Solvers

Traditional methods employ numerical techniques such as finite element methods (FEM), finite difference methods (FDM), finite volume methods (FVM), and pseudo-spectral methods (Grossmann, 2007; Šolín, 2005; Ciarlet, 2002; Courant et al., 1967; Cooley et al., 1969; Gottlieb & Orszag, 1977; Fornberg, 1998; Kopriva, 2009) to solve PDEs. These methods discretize the spatial domain, with higher precision requiring finer discretizations, which in turn increase computational costs. To reduce these costs, simplified models, such as Reynolds-averaged Navier-Stokes and large eddy simulations, have been proposed.

2.2. Learning-Based PDE Solvers

In recent developments, machine learning has emerged as a viable option for expediting simulations. The first group of PDE learners includes the PINN-based methods (Raissi et al., 2019; Lu et al., 2021b; Karniadakis et al., 2021) to take specific governing equation constraints as objective function terms (Yu et al., 2018; Wang et al., 2022; 2021). However, these methods struggle to generalize across different boundaries and initial conditions. Additionally, they

require prior knowledge of the dynamic system, including its equations, boundary conditions, and initial conditions, limiting their ability to learn directly from real-world data. Therefore, this paper will focus on Neural Operator methods and other state-of-the-art Transformer-based approaches.

Neural operator learning has recently become a heated topic within AI4Sci, where two main branches exist: DeepONet (Lu et al., 2021a) and Fourier Neural Operator (FNO) (Li et al., 2021), both proven to approximate any operator. DeepONet uses branch and trunk networks based on the universal approximation theorem (Chen & Chen, 1995), while FNO employs discrete Fourier transforms for kernel integral operators, offering a cost-accuracy trade-off due to quasi-linear complexity. This paper emphasizes Filter-based methods (Tran et al., 2023; Kossaifi et al., 2023; Xiong et al., 2024; Wen et al., 2022; Ashiqur Rahman et al., 2022; Raonic et al., 2024), including FNO and CNO. Other typical FNO-based methods include: Factorized FNO (F-FNO) (Tran et al., 2023) and Tensorized FNO (T-FNO) (Kossaifi et al., 2023). F-FNO is based on doing 1D Fourier transforms along axes respectively to reduce the number of parameters, while T-FNO focuses on using tensor factorizations (such as Tucker factorization). However, these works are not scalable to handle problems with multiple types of input functions. Another line of work (Cao, 2021) proposes to use the attention mechanism (Vaswani et al., 2017) for learning operators. CNO (Raonic et al., 2024) applies traditional convolution combined with interpolation upon a fixed finer resolution, so that the model could preserve the property of resolution-free as a neural operator.

Transformer-based methods have been long proven to be an effective module in many machine learning tasks (Katharopoulos et al., 2020; Schlag et al., 2021; Xiong et al., 2020; 2021; Shen et al., 2021; Nguyen & Salazar, 2019). Recent research has shown that this is also true for physics-simulation tasks. LSM (Wu et al., 2023) uses sine functions to approximate any function guaranteed by the theorem of Convergence of Trigonometric Approximation (Dyachenko, 1995), and utilizes an U-Net structure (Ronneberger et al., 2015) to handle multi-scale problems. GNOT (Hao et al., 2023), on the other hand, designed a novel heterogeneous normalized attention layer to handle the grids and input functions flexibly. Both of them have remarkable performances, but we are still not sure whether they can approximate any operators like DeepONet and FNO do (instead of merely approximating functions), so we put them in the category of Transformer-based methods.

3. DimOL

In this section, we present the technical details of a simple yet effective approach named dimension-aware operator learning (DimOL), which can be seamlessly integrated into

a wide range of neural operator-based PDE solvers. In Section 3.1, we initially introduce the general intuition behind DimOL. In Section 3.2, we propose a novel and lightweight neural network module named ProdLayer, which is motivated by dimensional awareness. In Section 3.3 and Section 3.4, we provide two specific implementations of using ProdLayer to replace the original neural network blocks in existing models, showing that DimOL is a universal technique applicable to various neural operator learning methods, adding negligible computational overhead.

3.1. Intuition of Dimensional Awareness

Dimensional awareness is a methodology that involves recognizing and incorporating the intrinsic dimensions and units of physical quantities into the design of AI models. This approach ensures that the model respects the physical laws governing the system, leading to more accurate and generalizable predictions. We believe that dimensional awareness would be a new dimension that we must consider when designing a new model for physical simulation.

In the context of solving PDEs, dimensional awareness allows the model to explicitly encode relationships and interactions between different physical quantities. For instance, in many physical systems, variables are often related through products and ratios that have specific dimensional properties. Traditional AI models may overlook these crucial relationships, leading to suboptimal results. In contrast, by encoding these product terms into the neural network, the model can better capture the underlying physics of the system, resulting in improved performance and generalization.

Below, we will use an example to briefly demonstrate why simply encoding product terms would improve model performance. Let's consider a classic prediction task in physics: predicting the future state of a physical field given its current state. The goal is to input a field of a physical quantity at a given moment and predict the same field after a certain period. This system is governed by a dynamic equation, often expressed as:

$$\frac{d}{dt} \mathbf{u}(\mathbf{x}, t) = \mathcal{G} \mathbf{u}(\mathbf{x}, t), \quad (1)$$

where \mathcal{G} is the time-evolution operator. In real-life situations, \mathcal{G} frequently appears as a summation of products, with each product term involving physical quantities of different dimensions. Despite the differing dimensions of the quantities involved, the resulting product terms share the same dimension as $\frac{d}{dt} \mathbf{u}(\mathbf{x}, t)$. For instance, consider the Navier-Stokes equations (Temam, 2001), which describe the motion of fluid substances. The governing equation for the Navier-Stokes problem is:

$$\rho \frac{d}{dt} \mathbf{v} = -\rho \mathbf{v} \cdot \nabla \mathbf{v} - \nabla p + \mu \nabla^2 \mathbf{v} + \rho \mathbf{f}, \quad (2)$$

where ρ is the fluid density, \mathbf{v} is the velocity field, p is the pressure field, μ is the dynamic viscosity, and \mathbf{f} is the external force field. In this equation, the left-hand side $\rho \frac{d}{dt} \mathbf{v}$ represents the rate of change of momentum per unit volume. On the right-hand side, we see a summation of terms involving products of physical quantities, where $\rho \mathbf{v} \cdot \nabla \mathbf{v}$ is the advection term, representing the transport of momentum, ∇p is the pressure gradient term, $\mu \nabla^2 \mathbf{v}$ is the diffusion term, and $\rho \mathbf{f}$ is the external force term. Each term on the right-hand side involves different combinations of physical quantities, yet all terms conform to the dimension of force per unit volume, matching the left-hand side.

Classic high-accuracy numerical methods, such as implicit Runge-Kutta methods, are often used to approximate time evolution in physical systems. These implicit methods involve numerous iterative steps to minimize the error within an acceptable tolerance, making them much slower compared to learning-based methods. On the other hand, explicit numerical methods, like the Forward Euler and explicit Runge-Kutta methods, are much faster. These methods involve straightforward calculations of the time-evolution operator \mathcal{G} for a finite number of times. Although explicit methods are computationally efficient, they can be less accurate and stable compared to implicit methods, especially for stiff equations or long-term integration. With our basic intuition, we would expect our neural operator learning method to at least have the capability to simulate explicit numerical methods effectively. Fortunately, the neural networks could do better than that since the training dataset is generated with implicit methods and even real-world data. As a result, while the models might simulate explicit methods in computational efficiency, they can also achieve the high accuracy and robustness typically associated with implicit methods.

If the objective of the learning-based models is to perform well across a wide range of input data distributions, the most straightforward approach is to enable the model to directly regress polynomial-structured terms. If the model is implemented correctly, it should be robust to variations in input scale and distribution. Our research demonstrates that dimension-aware models significantly outperform traditional models under such conditions. These models are inherently better at maintaining accuracy, even when inputs are scaled by large constants.

Another intuition comes from the Separation of Variables Method, a powerful technique commonly used in PDE analysis. Let's consider the 1D heat equation as an example:

$$\frac{\partial u}{\partial t} - \alpha \frac{\partial^2 u}{\partial x^2} = 0. \quad (3)$$

When using the Separation of Variables method, the solution

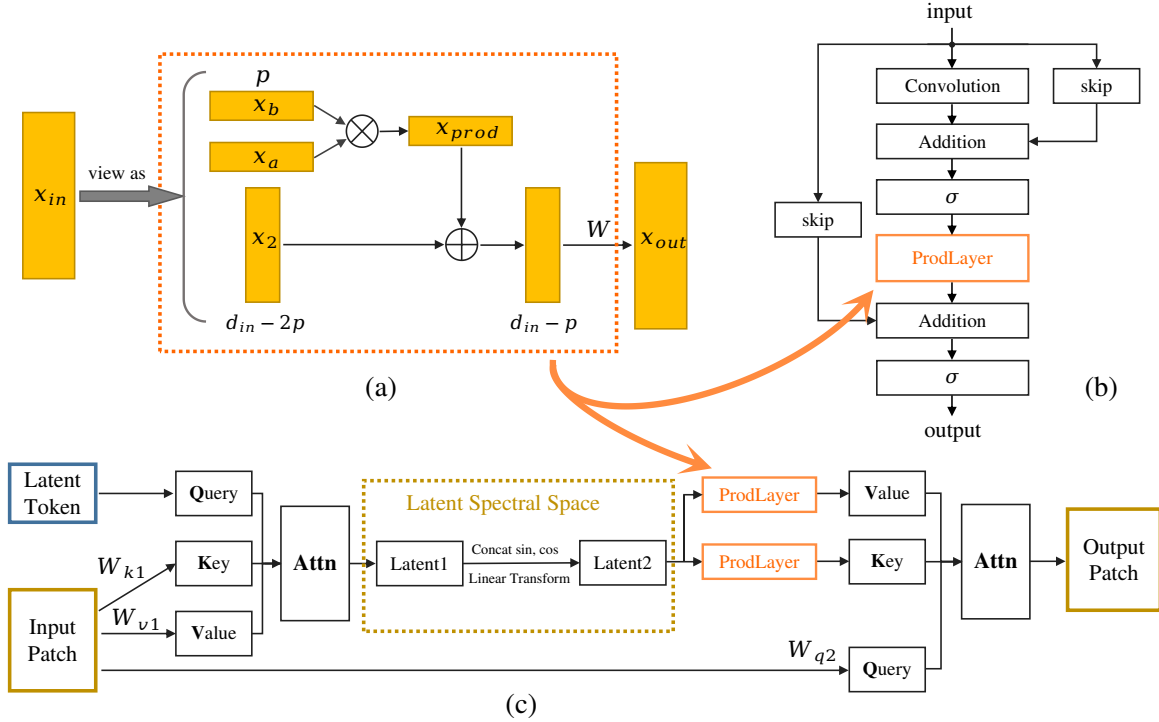


Figure 1. An illustration of our approach. **a**, ProdLayer directly encodes product terms by element-wise multiplication of \mathbf{x}_a and \mathbf{x}_b , followed by concatenation with \mathbf{x}_2 and a linear transformation. **b&c**, We integrate ProdLayer in existing FNO/CNO-based models (as a substitution of the original MLPs) and Transformer-based models like LSM (as additional modules with negligible extra parameters).

can be expressed as:

$$\begin{aligned} u(x, t) &= \sum_{n=1}^{\infty} D_n X(x) T(t) \\ &= \sum_{n=1}^{\infty} D_n \sin \frac{n\pi x}{L} \exp \left(-\frac{n^2 \pi^2 \alpha t}{L^2} \right). \end{aligned} \quad (4)$$

This solution exactly takes the form of a sum-of-products, where $X(x)$ and $T(t)$ are the spatial and temporal components, respectively, and D_n are the coefficients. This form is highly amenable to learning-based approaches, as it suggests that the model can effectively learn to regress these coefficients and basis functions.

3.2. ProdLayer: Integrating DimOL Product Terms

To encode product terms in a neural network, the most straightforward approach is to directly multiply two terms. This leads us to the design of ProdLayer, which can be integrated into the model to handle such operations efficiently. Let's define the input vector \mathbf{x} as follows:

$$\mathbf{x} = \mathbf{x}_a \oplus \mathbf{x}_b \oplus \mathbf{x}_2, \quad (5)$$

where \oplus denotes feature concatenation, \mathbf{x}_a and \mathbf{x}_b are sub-vectors with the same dimensionality, *i.e.*, $\dim(\mathbf{x}_a) = \dim(\mathbf{x}_b) = p$, and p denotes the number of product terms.

ProdLayer operates as follows:

$$\sigma_{\text{prod}}(\mathbf{x}) = W [(\mathbf{x}_a \otimes \mathbf{x}_b) \oplus \mathbf{x}_2], \quad (6)$$

where \otimes denotes the element-wise product and W represents a learnable weight matrix. This formulation allows the layer to directly incorporate the product terms of \mathbf{x}_a and \mathbf{x}_b , combined with additional input features \mathbf{x}_2 . The structure of ProdLayer is shown in Figure 1(a).

Another simple way to introduce product terms is by using the identity $ab = \frac{1}{4}[(a+b)^2 - (a-b)^2]$, which expresses the product as the difference of two square terms. However, within the TorusLi experiment, as shown in Table 3, this indirect method of encoding product terms is demonstrated to be less effective than ProdLayer.

The mechanism of ProdLayer allows the neural network to capture and encode the product terms directly, leveraging the physical intuition behind polynomial structures and product terms found in many dynamic systems governed by PDEs. By incorporating ProdLayer, the model can effectively learn and represent these relationships, improving its performance on tasks with a wide range of input data distributions.

3.3. Filter-Based Models with ProdLayer

For filter-based models, namely, FNO-based models and CNO, introducing product-term encoding via ProdLayer enables the model to approximate explicit numerical meth-

ods more accurately. This is particularly beneficial when the evolution operator takes the form of sum-of-products, a common scenario in complex dynamic systems. As shown in Figure 1(b), we replace the MLP in the base model with ProdLayer. This modification allows the model to directly encode product terms, enhancing its ability to capture the intrinsic relationships between physical quantities.

In our implementation of FNO models, we adopt the backbone of the T-FNO. This choice offers the flexibility to switch between using tensor factorization and the original FNO, providing a versatile framework for experimentation. When tensor factorization is not used, the model functions as a standard FNO. We demonstrate the effectiveness of our approach by presenting uniformly enhanced performance with ProdLayer. By analyzing the Fourier weights, we provide insights into how the network conceptualizes the physical quantities involved. This analysis is especially insightful in the context of a toy example related to the Burgers equation, which is discussed in Section 4.8.

3.4. Transformer-Based Models with ProdLayer

LSM is a cutting-edge Transformer-based model designed for solving PDEs. Its basic innovation is the incorporation of Sine functions into the network, allowing it to approximate any (periodic) function within a specific spectral range. For non-periodic components, LSM utilizes convolution-based neural blocks. The overall structure of LSM is akin to a U-Net, enabling it to learn interactions between different patches of the domain at varying scales.

Inspired by the separation of variables method, we hypothesize that the projection in the latent spectral space can be enhanced if terms can multiply Sine or Cosine functions directly, rather than merely adding them as biases. This modification aligns with the core principle of DimOL, which aims to improve model performance by encoding product terms. To implement this idea, we replace the linear transformation in the decoder of LSM with a ProdLayer, as shown in Figure 1(c). This enhanced architecture retains the original strengths of LSM while integrating ProdLayer allows the model to handle product terms more effectively. Given this intuition, a larger number of product terms for each ProdLayer is beneficial and can enhance the model’s capacity to capture complex interactions.

4. Experiments

4.1. Experimental Setups

We apply DimOL to multiple base models and evaluate their performance in a variety of settings, including both regular mesh settings (Burgers, Darcy Flow, Navier-Stokes) and irregular mesh settings (Inductor2D). Notably, DimOL does not apply to geometry-only datasets. In these datasets, the

Table 1. Prediction results on the Burgers dataset. We use ProdLayer in the DimOL methods and show that our approach consistently improves the performance of the base models.

Model	# Param	MSE (10^{-3})	Gain
FNO (2021)	0.098M	1.683	-
FNO + DimOL	0.105M	1.428	9.3%
T-FNO (2021)	0.052M	2.225	-
T-FNO + DimOL	0.056M	1.147	48.4%
CNO (2024)	1.928M	73.255	-
CNO + DimOL	1.912M	64.684	11.7%

inputs consist solely of coordinates, which lack the physical dimensions that DimOL leverages. Thus, there is no dimensional information for DimOL to exploit. However, this does not imply that DimOL would fail on irregular meshes. The GNOT paper introduced the Inductor2D dataset, which includes physical quantities as part of the input. This allows us to test the model’s generalization ability to real-world scenarios where background physical conditions could change.

For the Burgers, Darcy Flow, and Navier-Stokes datasets, we test DimOL on several neural operator models, including FNO, F-FNO, T-FNO, and LSM. These models were chosen due to their effectiveness in handling PDEs across different settings. As for Inductor2D, we adapt the GNOT model with DimOL. The models we use are 4-layer models.

The following experiments use a product number of $p = 2$ in each ProdLayer (see Figure 1). While this empirical value may not be the optimal solution for every specific dataset, it consistently leads to improvements in our experiments. Other options for the p value also yield performance improvements and are discussed in Appendix B. Specifically, setting $p = 0$ would reduce the channel-mixing layer of the model to an ordinary MLP. For FNO and LSM models, we adopt the original depth settings of 4 layers.

4.2. Burgers

We adopt the 1D Burgers dataset of the FNO paper, which can be described using the following equation: $\partial_t u(x, t) + u(x, t) \partial_x(u(x, t)) = \nu \partial_{xx} u(x, t)$, $x \in (0, 1)$, $t \in (0, 1]$. Since this is a 1D problem, more complex methods like F-FNO, T-FNO, and LSM are not applicable, so we compare FNO with its dimension-aware counterpart, FNO + ProdLayer. As shown in Table 1, we evaluate the 4-layer T-FNO models on the Burgers dataset and achieve an impressive 48.4% drop in MSE on the test set, which performs the best; the adapted FNO model also achieves a gain of 9.3% on Burgers dataset. Similar effects also hold for CNO models.

4.3. Darcy Flow

This dataset is also sourced from FNO. The physical process of Darcy Flow can be described by the equation

Table 2. Prediction results on the Darcy Flow dataset. The use of DimOL provides consistent performance gains.

Model	# Param	MSE (10^{-3})	Gain
FNO (2021)	1.658M	5.889	-
FNO + DimOL	1.663M	5.726	2.8%
T-FNO (2023)	0.684M	7.500	-
T-FNO + DimOL	0.682M	6.919	7.8%
LSM (2023)	4.813M	2.892	-
LSM + DimOL	4.812M	2.713	6.2%
CNO (2024)	5.582M	9.525	-
CNO + DimOL	5.578M	8.773	7.9%

Table 3. Prediction results on the TorusLi dataset. We conduct experiments with alternative architectures to implement DimOL.

Base model	DimOL	MSE	Gain
FNO	-	0.1496	-
FNO	QuadLayer	0.1431	4.3%
FNO	ProdLayer	0.1394	6.8%
T-FNO	-	0.1448	-
T-FNO	QuadLayer	0.1430	1.2%
T-FNO	ProdLayer	0.1404	2.3%
F-FNO	-	0.1651	-
F-FNO	ProdLayer	0.1542	6.6%
CNO	-	0.2044	-
CNO	ProdLayer	0.1893	7.4%

$-\nabla \cdot (a(x)\nabla u(x)) = f(x)$, $x \in (0, 1)^2$, where the input is $a(x)$ and the output is $u(x)$, which satisfies the steady-state equation. Notably, this setting focuses on finding a steady state under given conditions, differing from dynamic prediction tasks. As shown in Table 2, the DimOL-adapted models consistently outperform the original versions.

4.4. Navier-Stokes

The TorusLi dataset is introduced by the original FNO paper. The governing equation is as follows: $\frac{\partial \omega}{\partial t} + \mathbf{u} \cdot \nabla \omega = \nu \nabla^2 \omega + f$, $\nabla \cdot \mathbf{u} = 0$, $\nabla \times \mathbf{u} = w \mathbf{e}_z$. The input is the initial vorticity $\omega_0(x, y) = \omega(x, y, t = 0)$, while the external force term is fixed within the dataset. A main drawback of the TorusLi dataset: is lacking the diversity of other variables. To resolve this, F-FNO (Tran et al., 2023) introduces the TorusVisForce dataset. The core idea is to ensure that the model is general enough to handle varying environmental conditions, such as different external force terms and viscosity coefficients. To achieve this, these terms are set as random during dataset generation and are used as inputs for the model. Additionally, FNO conducts TorusLi experiments using a sequence of previous fluid fields (e.g., 10 steps). F-FNO suggests that this task should adhere to the first-order Markov property, meaning that one time step is sufficient. We adopt this setting, which may explain why LSM does not outperform FNO methods here, contrary to

Table 4. Prediction results ($\times 10^{-2}$) on the TorusVisForce dataset. T denotes different prediction time horizons.

Model	$T = 4$		$T = 10$	
	MSE	Gain	MSE	Gain
T-FNO (2023)	1.090	-	1.717	-
T-FNO + DimOL	0.966	11.5%	1.622	5.5%
CNO (2024)	3.457	-	6.264	-
CNO + DimOL	3.308	4.3%	5.838	6.8%

Table 5. MSE on the Inductor2D dataset with irregular meshes. We use GNOT as the baseline model here, as other compared methods did not include this dataset in their original papers.

Model	$A_z (10^{-2})$	B_x	B_y	Gain
GNOT (2023)	0.8736	0.2579	0.3873	-
GNOT + DimOL	0.8869	0.2578	0.3847	4.8%

the findings reported in the LSM paper.

TorusLi. As shown in Table 3, DimOL models consistently outperform the base models on the TorusLi dataset. Additionally, we test the product term encoding with quadratic layers. However, as demonstrated in the tests on FNO and T-FNO, the quadratic layer does not surpass the performance of the more straightforward ProdLayer.

TorusVisForce. Due to the size of the TorusVisForce dataset, we select T-FNO for our case study, given its strong performance on TorusLi. In the TorusVisForce dataset, the involvement of more physical quantities in the input allows the DimOL models to achieve significant improvements. We conduct two tasks: in the first, we set the prediction horizon to $T = 4$ time steps, while in the second, we have $T = 10$. Obviously, as the prediction horizon extends, the task becomes more challenging. Table 4 presents the prediction errors. We observe that DimOL significantly improves the performance of the base models in both tasks.

4.5. Inductor2D

The datasets mentioned above primarily involve regular meshes. What about irregular meshes? One might suggest checking out Geo-FNO’s Airfoil, Pipe, and Elasticity datasets. However, does dimensional awareness truly apply here? These datasets are mesh-only and lack any physical quantities as inputs! Moreover, the datasets are pretty weird by making all the meshes outside the boundaries also a part of the input. They’re merely redundant “auxiliary lines” that are used to generate the dataset, and no matter how they twist, the boundary would remain the same. This can confuse the model, leading to inconsistent outputs. Therefore, we adopt the Inductor2D dataset introduced by GNOT.

In our implementation, the adaptation with GNOT is similar to how we adapted LSM, specifically by replacing the decoder’s linear projections with ProdLayers. We do not

Table 6. OOD few-shot learning results in MSE ($\times 10^{-2}$) on TorusVisForce ($T = 4$). Here, p is the hyperparameter in ProdLayer and k denotes the scaling coefficient applied to the in-set physical quantities to construct OOD data.

Base	DimOL	In-Set	OOD ($k = 4$)	OOD ($k = 16$)
T-FNO	-	2.354	1.158	1.246
T-FNO	$p = 0$	1.625	1.005	1.062
T-FNO	$p = 2$	1.456	0.911	0.984
	Gain		10.4%	9.4%
				7.3%
LSM	$p = 0$	8.304	1.427	1.500
LSM	$p = 2$	8.031	1.262	1.334
	Gain		3.3%	11.6%
				11.1%

perform any hyperparameter search. The model follows the default hyperparameters of GNOT: the hidden dimension is 64, and the number of attention heads is set to 8. As illustrated in Table 5, we achieve improved results by simply applying DimOL with the number of products set to $p = 1$.

4.6. Out-of-Distribution Few-Shot Learning Studies

We aim to develop a model that approximates an operator while preserving the key properties of the original operator. If successful, the model should generalize well in few-shot learning scenarios. To evaluate this, we design the following experiments. We construct a subset of the TorusVisForce dataset, containing 200 data sequences with viscosity ranging in $[8.2 \times 10^{-5}, 1 \times 10^{-4}]$. For few-shot learning, we use 100 random samples from this dataset as the training set. We employ two test settings:

- *In-set test*: We first perform in-distribution testing on the other partition of 100 unseen samples.
- *OOD test*: We generate an OOD test set by scaling the in-set test data using a coefficient k , where k is an integer applied to the physical quantities ω , f , and ν .

For *OOD* testing, we leverage a crucial principle from dimensional analysis: the invariance of similar transformations. This principle motivates us to create *partially out-of-distribution* test data using simple data transformations to assess operator learning. The transformed data, while indeed outside the original data distribution, effectively maintains similar dynamics to the training data. We use the TorusVisForce dataset as a case study. Consider data transformations:

$$\omega_0 \rightarrow k\omega_0, \quad t \rightarrow t/k, \quad \nu \rightarrow k\nu, \quad f \rightarrow k^2 f. \quad (7)$$

If we scale the inputs, the output should adhere to the following relationship:

$$\omega_{\text{new}}(x, T_{\text{new}} = T/k) = k\omega(x, T), \quad (8)$$

which is validated using a traditional numerical solver, although a slight numerical bias is observed. Therefore,

in the OOD experiments, although DimOL cannot access the analytic expression for the actual operator $G^\dagger : [H_{\text{per}}^r((0, 1)^2), L_{\text{per}}^2((0, 1)^2; \mathbb{R}), \mathbb{R}_+] \rightarrow H_{\text{per}}^r((0, 1)^2)$ in TorusVisForce, it will seek to uncover the key properties from the transformed data.

Table 6 reveals the impressive few-shot learning capability of DimOL models. More significantly, it highlights the acquisition of a similar-transformation invariance property, which scientists may anticipate from the ground-truth operator. This property is particularly beneficial when combining machine learning with traditional dimensional analysis.

4.7. Generalization to New Boundary Conditions

Another profound issue of machine-learning-based PDE solvers is how well they can generalize across different boundaries. In this work, we employ the cylinder-flow setting. In this setting, we consider cylinders of various shapes randomly placed within the domain, and we impose the Dirichlet Boundary Condition on the velocity field. The domain has open boundaries on the left and right sides, while the upper and lower sides act as closed boundaries. The initial condition specifies a zero-velocity field throughout the domain, except on the left side where the velocity is set to v_0 . Soon after the fluid flow encounters the cylinder, the velocity field develops a pattern of Karman Vortex Street.

Our datasets consist of cylinders with different shapes: Shape C represents a circle, S represents a square, and T represents a triangle. We train the models on a training set with four types of boundary conditions: (1-3) 1C, 1S, and 1T, simulating flows with a single circle, square, and triangle, respectively; and (4) ST, which includes one square and one triangle. The test data includes cylinders of in-set boundaries 1C, 1S, 1T, and ST, as well as out-of-distribution (OOD) combinations of CS and CT. Given that reflections can occur between two cylinders, making accurate predictions on test sets with two-cylinder problems is challenging. However, since the model is trained on individual shapes C, S, and T, along with the combination ST, it is expected to generalize well to the unseen combinations CS and CT.

For this experiment, only FNO-based models are suitable for the rectangular domain. Therefore, we select FNO and T-FNO as our baseline models. As shown in Table 7, the DimOL models not only outperform the baseline models on the in-set datasets but also demonstrate excellent generalizability under unseen boundary conditions. A representative case is presented in Figure 2.

4.8. Finding New Physical Terms with DimOL

Symbolic regression has long been a prominent topic in AI for Science, yet combining symbolic methods with neural networks remains a challenge. Symbolically regressing a

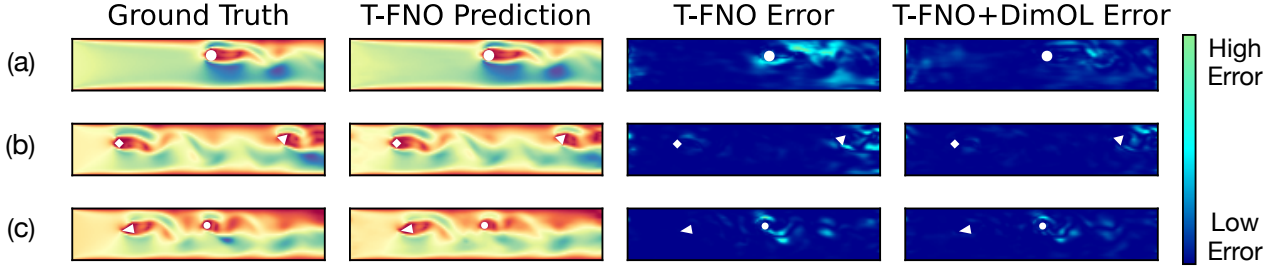


Figure 2. Heatmap of predicted velocity and corresponding errors under different boundary conditions, which can be different from those in the training data. We have 3 types of cylinders: Circle, Square, and Triangle. (a): Task 1C — single Circle; (b): Task ST — one Square and one Triangle; (c): Task CT — one Circle and one Triangle. Notably, we train the models on four tasks: 1C, 1S, 1T, and ST. Therefore, (a) and (b) represent in-set test cases, while (c) represents OOD samples.

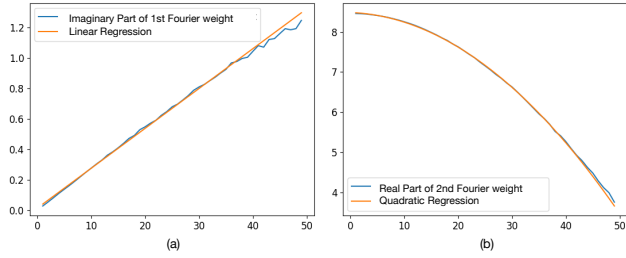


Figure 3. Results of regressed spectral terms. (a) The imaginary part of the 1st Fourier weight, *i.e.*, the linear term. (b) The real part of the 2nd Fourier weight, *i.e.*, the quadratic term.

specific function is already complex, let alone regressing operators. However, by incorporating dimensional awareness, a network can gradually identify meaningful physical terms. Below, we present a toy example illustrating how we derive the evolution operator for the Burgers equation. The model is structured as follows: 1) A Fourier Layer; 2) A residual connection to a convolution layer; 3) A ProdLayer. Visualizing the weights of the Fourier layer reveals terms like k and k^2 , which correspond to the first and second derivatives obtained through Fourier transforms:

$$\begin{aligned} \frac{d}{dx}g(x) &= \mathcal{F}^{-1}[ik(\mathcal{F}g(x))], \\ \frac{d^2}{dx^2}g(x) &= \mathcal{F}^{-1}[-k^2(\mathcal{F}g(x))]. \end{aligned} \quad (9)$$

These two operators correspond to the -1 and -2 orders of the length dimension. Traditional FNO models struggle with shallower layers. Even with a parameter count increased to 1.25 million, they often suffer from severe overfitting and fail to learn the actual operator, despite achieving reasonable performance. In contrast, improving FNO with DimOL achieves significantly better results with just a thousand parameters. The minimum MSE on the validation set are 0.0227 for FNO and 0.0137 for FNO+DimOL, which means the FNO+DimOL can reduce the error by 39.6%.

As is shown in Figure 3, the first Fourier expression we regressed is the imaginary part: $f(k) = 0.02618k + 0.01474$, achieving a Pearson correlation of 0.999. The second

expression, representing the real part, is $-0.001907k^2 + 0.01474k + 8.482$, with a Pearson correlation of 0.9999.

5. Conclusions and Limitations

In this paper, we introduced DimOL as an adaptation for major models tailored to solving high-dimensional PDEs. These include Filter-based models (FNO and CNO) and Transformer-based models such as LSM and GNOT. We discovered that dimensional awareness not only makes sense for human physicists but also machine learning models, especially when the task involves actual physical quantities as input. Our research indicates that this conclusion applies across a wide range of models and datasets. By enhancing the model’s symbolic meaning, DimOL models are better suited for reverse engineering to uncover terms with potential physical significance. While we currently use ProdLayer for DimOL, we believe that DimOL is more than this. It should be regarded as a new “dimension” to consider when designing AI4Sci models.

Notably, fully quantifying and interpreting the profits of considering dimensional awareness as a property of a model remains an open problem. One approach is to apply the model to simpler, more comprehensible datasets, such as the evolution operator for the Burgers equation in Section 4.8. This allows for identifying which dimensions are associated with the ProdLayer by analyzing the Fourier weights. However, for more complex datasets, the relationships among the Fourier weights may not have clear symbolic interpretations, making it difficult to analyze their internal connections. Therefore, it is more appropriate to view dimensional awareness as a novel and effective design principle for neural operators, rather than as a definitive scientific claim about a model’s capacity to perceive dimensions.

Another potential limitation of DimOL is its effectiveness in tasks where the input data lacks clear dimensional information or where the relationship between dimensions is highly complex or nonlinear. In these cases, DimOL may not provide substantial improvements.

Impact Statement

The potential applications and social impact of deep learning-based PDE Neural Operators (including DimOL) are vast, as they can revolutionize many fields that rely on solving complex differential equations. By leveraging deep learning to solve PDEs, these models can significantly accelerate scientific discovery, improve engineering designs, and enhance decision-making in real-world systems. Particularly for DimOL, it can universally enhance the performance of Neural Operators. By incorporating dimensional awareness into both Filter-based models (such as FNO and CNO) and Transformer-based models (including LSM and GNOT), our approach enables these models to more effectively capture the underlying physical relationships. Through the analysis of Fourier components' weights, DimOL can symbolically discern the physical significance of each term in the model. This is exemplified in the case of the Burgers equation, where the model can identify terms corresponding to derivatives. This interpretability is crucial as it allows physicists and engineers to better understand how neural networks model physical phenomena.

While learning-based PDE solvers have the potential to accelerate and enhance simulations of complex physical systems, there are potential negative social impacts to consider. These issues largely stem from data bias, the way these methods could be deployed, and ethical concerns related to their use. For example, if the training data is skewed or incomplete (for instance, if it predominantly comes from specific environments, regions, or conditions), the model could generate inaccurate or overly generalized predictions for real-world applications.

References

Ashiqur Rahman, M., Ross, Z. E., and Azizzadenesheli, K. U-no: U-shaped neural operators. *arXiv e-prints*, pp. arXiv–2204, 2022.

Cao, S. Choose a transformer: Fourier or galerkin. *Advances in neural information processing systems*, 34: 24924–24940, 2021.

Chen, T. and Chen, H. Universal approximation to nonlinear operators by neural networks with arbitrary activation functions and its application to dynamical systems. *IEEE transactions on neural networks*, 6(4):911–917, 1995.

Ciarlet, P. G. *The finite element method for elliptic problems*. SIAM, 2002.

Cooley, J. W., Lewis, P. A., and Welch, P. D. The fast fourier transform and its applications. *IEEE Transactions on Education*, 12(1):27–34, 1969.

Courant, R., Friedrichs, K., and Lewy, H. On the partial difference equations of mathematical physics. *IBM journal of Research and Development*, 11(2):215–234, 1967.

Dyachenko, M. The rate of u-convergence of multiple fourier series. *Acta Mathematica Hungarica*, 68(1-2): 55–70, 1995.

Fornberg, B. *A practical guide to pseudospectral methods*. Cambridge university press, 1998.

Gottlieb, D. and Orszag, S. A. *Numerical analysis of spectral methods: theory and applications*. SIAM, 1977.

Grossmann, C. *Numerical treatment of partial differential equations*. Springer, 2007.

Hao, Z., Wang, Z., Su, H., Ying, C., Dong, Y., Liu, S., Cheng, Z., Song, J., and Zhu, J. Gnot: A general neural operator transformer for operator learning. In *ICML*, 2023.

Karniadakis, G. E., Kevrekidis, I. G., Lu, L., Perdikaris, P., Wang, S., and Yang, L. Physics-informed machine learning. *Nature Reviews Physics*, 3(6):422–440, 2021.

Katharopoulos, A., Vyas, A., Pappas, N., and Fleuret, F. Transformers are rnns: Fast autoregressive transformers with linear attention. In *International conference on machine learning*, pp. 5156–5165. PMLR, 2020.

Kopriva, D. A. *Implementing spectral methods for partial differential equations: Algorithms for scientists and engineers*. Springer Science & Business Media, 2009.

Kossaifi, J., Kovachki, N., Azizzadenesheli, K., and Anandkumar, A. Multi-grid tensorized fourier neural operator for high-resolution pdes. In *arxiv*, 2023.

Li, Z., Kovachki, N. B., Azizzadenesheli, K., Liu, B., Bhattacharya, K., Stuart, A., and Anandkumar, A. Fourier neural operator for parametric partial differential equations. In *International Conference on Learning Representations*, 2021. URL <https://openreview.net/forum?id=c8P9NQVtmnO>.

Lu, L., Jin, P., Pang, G., Zhang, Z., and Karniadakis, G. E. Learning nonlinear operators via deeponet based on the universal approximation theorem of operators. *Nat. Mach. Intell.*, 2021a.

Lu, L., Meng, X., Mao, Z., and Karniadakis, G. E. Deepxde: A deep learning library for solving differential equations. *SIAM review*, 63(1):208–228, 2021b.

Nguyen, T. Q. and Salazar, J. Transformers without tears: Improving the normalization of self-attention. *arXiv preprint arXiv:1910.05895*, 2019.

Raissi, M., Perdikaris, P., and Karniadakis, G. E. Physics-informed neural networks: A deep learning framework for solving forward and inverse problems involving nonlinear partial differential equations. *J. Comput. Phys.*, 2019.

Raonic, B., Molinaro, R., De Ryck, T., Rohner, T., Bartolucci, F., Alafari, R., Mishra, S., and de Bézenac, E. Convolutional neural operators for robust and accurate learning of pdes. *Advances in Neural Information Processing Systems*, 36, 2024.

Ronneberger, O., Fischer, P., and Brox, T. U-net: Convolutional networks for biomedical image segmentation. In *Medical image computing and computer-assisted intervention—MICCAI 2015: 18th international conference, Munich, Germany, October 5–9, 2015, proceedings, part III* 18, pp. 234–241. Springer, 2015.

Schlag, I., Irie, K., and Schmidhuber, J. Linear transformers are secretly fast weight programmers. In *International Conference on Machine Learning*, pp. 9355–9366. PMLR, 2021.

Shen, Z., Zhang, M., Zhao, H., Yi, S., and Li, H. Efficient attention: Attention with linear complexities. In *Proceedings of the IEEE/CVF winter conference on applications of computer vision*, pp. 3531–3539, 2021.

Šolín, P. *Partial differential equations and the finite element method*. John Wiley & Sons, 2005.

Temam, R. *Navier-Stokes equations: theory and numerical analysis*, volume 343. American Mathematical Soc., 2001.

Tran, A., Mathews, A., Xie, L., and Ong, C. S. Factorized fourier neural operators. In *ICLR*, 2023.

Vaswani, A., Shazeer, N., Parmar, N., Uszkoreit, J., Jones, L., Gomez, A. N., Kaiser, Ł., and Polosukhin, I. Attention is all you need. *Advances in neural information processing systems*, 30, 2017.

Wang, S., Teng, Y., and Perdikaris, P. Understanding and mitigating gradient flow pathologies in physics-informed neural networks. *SIAM Journal on Scientific Computing*, 43(5):A3055–A3081, 2021.

Wang, S., Yu, X., and Perdikaris, P. When and why pinns fail to train: A neural tangent kernel perspective. *Journal of Computational Physics*, 449:110768, 2022.

Wen, G., Li, Z., Azizzadenesheli, K., Anandkumar, A., and Benson, S. M. U-fno—an enhanced fourier neural operator-based deep-learning model for multiphase flow. *Advances in Water Resources*, 163:104180, 2022.

Wu, H., Hu, T., Luo, H., Wang, J., and Long, M. Solving high-dimensional pdes with latent spectral models. In *ICML*, 2023.

Xiong, R., Yang, Y., He, D., Zheng, K., Zheng, S., Xing, C., Zhang, H., Lan, Y., Wang, L., and Liu, T. On layer normalization in the transformer architecture. In *International Conference on Machine Learning*, pp. 10524–10533. PMLR, 2020.

Xiong, W., Huang, X., Xu, Y., Sun, J., He, W., Tan, Z., Cheng, A., Weng, K., Qiu, Y., Wang, Y., et al. Koopman neural operator for learning non-linear partial differential equations. *Journal of Computational Physics*, 2024.

Xiong, Y., Zeng, Z., Chakraborty, R., Tan, M., Fung, G., Li, Y., and Singh, V. Nyströmformer: A nyström-based algorithm for approximating self-attention. In *Proceedings of the AAAI Conference on Artificial Intelligence*, volume 35, pp. 14138–14148, 2021.

Yu, B. et al. The deep ritz method: a deep learning-based numerical algorithm for solving variational problems. *Communications in Mathematics and Statistics*, 6(1):1–12, 2018.

Appendix

A. Quantitative Generalization Results on New Boundary Conditions

The experiment results for Section 4.7 are recorded in Table 7.

Table 7. Prediction MSE ($\times 10^{-2}$) on the CylinderFlow dataset under different boundary conditions We have 3 types of cylinders: Circle, Square, and Triangle. We train the models on four tasks: 1C (one circle), 1S (one square), 1T (one triangle), and ST (one square and one triangle). Therefore, CS and CT represent OOD test cases.

Model	A	B	C	BC	AB	AC	Gain (In-Set)	Gain (OOD)
FNO	4.358	5.720	4.885	12.93	12.16	11.82	-	-
FNO + ProdLayer	3.998	5.403	4.622	12.38	11.85	11.16	4.488%	4.016 %
T-FNO	4.059	5.231	4.501	12.23	11.55	10.91	-	-
T-FNO + ProdLayer	3.881	5.192	4.472	0.1194	11.28	10.17	2.156%	4.505%

B. Hyperparameter Sensitivity Analyses

All the experiments presented earlier used a product term number of $p = 2$. What about other p values and models without any channel mixing? In Table 8, we find that all models with ProdLayer at $p = 2$ consistently outperform the $p = 0$ cases (*i.e.*, MLP). The performance does not necessarily improve with the growth of p value; instead, the key factor is whether we employ ProdLayer for channel mixing. Additionally, we observe from Table 8 that if channel mixing with an MLP layer is beneficial, replacing the linear layers with ProdLayer yields even better performance. However, in some cases, such as in the Burgers experiments, adding channel mixing to the original model does not guarantee improvement and may lead to the overfitting problem.

Table 8. Hyperparameter sensitivity analyses on the choice of p used in ProdLayer. Results are presented in MSE ($\times 10^{-3}$). For TorusLi, we set the prediction horizon to $T = 10$. For TorusVisForce, we conduct the few-shot experiments with $N = 100$ and $T = 4$.

Dataset	Base Model	Base Result	$p = 0$	$p = 1$	$p = 2$	$p = 4$	$p = 8$	$p = 16$
Burgers	T-FNO	2.225	2.342	1.130	1.147	1.163	1.059	1.071
Darcy Flow	LSM	2.892	2.892	2.823	2.713	2.632	2.716	2.720
TorusLi	T-FNO	0.1448	0.1425	0.1396	0.1404	0.1384	0.1398	0.1398
TorusVisForce	T-FNO	2.037	2.104	1.759	1.757	1.733	1.752	1.690